Kinetic analysis of particle-size based complex kinetic processes

Roman Svoboda*

Department of Physical Chemistry, University of Pardubice, Studentska 573, 532 10 Pardubice, Czech Republic

Abstract

Complex kinetic data arbitrarily created by measuring (calorimetrically) crystallization of mixed selenium powders with different defined particle sizes were evaluated by the three standard approaches to complex kinetic analysis. Performance of the three tested approaches was tested by comparison with the kinetic results obtained for the separate powder fractions. The additivity of the kinetic signals was verified. Single-process methods of kinetic analysis provided qualitative and quantitative information about the temperature dependence of activation energy E and estimation of the ratio between intensities of the involved sub-processes I_1/I_2. Mathematic deconvolution approach well reflected the correct model-free and model-based kinetics for the partial overlaps. However, it required iterative processing and additional supplemental information about the nature of the sub-processes in case of the evaluation of fully overlapping data. Kinetic deconvolution based on single-curve non-linear optimization utilizing the fixed E values obtained independently provided very good results for both, partial and full overlaps.

Keywords: complex kinetic analysis, particle size, DSC, selenium glass, deconvolution

* Corresponding author: Tel.: +420 466 037 346 E-mail address: roman.svoboda@upce.cz

1. Introduction

Deconvolution of complex kinetic processes (i.e. processes with several overlapping reaction mechanisms) is a hot topic in the field of kinetic analysis (KA) of solid-state processes. Numerous papers were published in this field, reporting mainly on the theory and implementation of various methodologies of KA [1 - 10], intricacies of the baseline subtraction [11, 12] or practical KA utilization in case of exemplary complex solid-state processes [13 - 20]. One of the main (but often forgotten) factors causing the process complexity is the wide distribution of particle sizes in the powdered material. Such influence of particle size on the process kinetics was recently studied in detail for the crystallization of several compositional families of chalcogenide glasses [21 - 30] but, in general, the influence of material powdering and the consequences of the rapid increase of crystallization rate due to the presence of mechanically induced defects [31] are often ignored in literature. This may have to do with the specificities of the crystallization complexity, namely with the often observed temperature-dependent kinetics [32] (kinetic parameters/models changing with applied heating rate q^+ and/or temperature range), that are difficult to describe by the traditional approaches to KA calculations and need to be solved via single-curve optimization [32].

In the present paper the arbitrarily created kinetic complexity based on purposefully mixed defined amounts of different fraction-sized powders will be studied by differential scanning calorimetry (DSC) with regard to the performance of the particular methods of KA in complex process scenarios. Pure selenium glass with well-known crystallization behavior [33 - 36] exhibiting single-peak kinetics for all powder size fractions will be used as a model material. It was already reported earlier [32] that crystallization from glassy matrices belongs among the processes with most intricate kinetic behavior, often exhibiting strong changes of kinetics with increasing temperature or heating rate. Selenium glass indeed shows such

behavior. [33 - 36] In addition, for the purpose of the present paper the kinetic complexity will be arbitrarily created to form both partial and full overlaps of the kinetic sub-peaks. This will push the testing of the nowadays complex-process KA methodologies to the highest level. Performance of the following methods of KA will be tested: isoconversional methods, mathematical deconvolution followed by single-peak kinetic analysis, kinetic deconvolution based on non-linear optimization. Moreover, the testing will be also focused on the potential additivity of the crystallization signals corresponding to the separate powder fractions when mixture of differently sized powders is measured.

2. Theory of complex process kinetic analysis

Theory of kinetic analysis revolves around the enumeration of the standard kinetic equation [37]:

$$d\alpha/dt = I \cdot A \cdot e^{-E/RT} \cdot f(\alpha) \quad (1)$$

where α is the degree of conversion, t is time, T is temperature, I is the integrated area under the kinetic peak (crystallization enthalpy in case of the present data), A is the pre-exponential factor, E is the apparent activation energy of the process, R is the universal gas constant and f(α) is the appropriate kinetic model function.

Evaluation tools of KA used for treating the complex process signals can be divided into three approaches. The first approach utilizes methods primarily developed for single-process reaction mechanisms (following Eq. 1) and interprets their results in the complex-process scenarios. The most famous group of methods falling in this category are the isoconversional methods determining the activation energy E in dependence on degree of conversion α. The isoconversional methods can be further split into two sub-groups – differential and integral methods, where each sub-group provides (due to the inherent procedural approach) different E-α dependence. It was recently shown in [38] that in case of

complex processes the various methods categorized within each respective sub-group of isoconversional methods provide extremely similar results, the interpretation of which is not influenced by the choice of the particular method. Therefore, in the present paper only one method from each sub-group will be used for evaluation of E-α dependences: the differential Friedman method [39] (Eq. 2) and the integral Starink method [40] (Eq. 3).

$$\ln\left(\left[d\alpha/dt\right]_\alpha\right) = -\frac{E}{RT_\alpha} + const. \tag{2}$$

$$\ln\left(\frac{q^+}{T_\alpha^{1.92}}\right) = -1.0008\frac{E}{RT_\alpha} + const. \tag{3}$$

where q^+ is heating rate, $(d\alpha/dt)_\alpha$ and T_α are the conversion rate and temperature corresponding to arbitrarily chosen values of conversion α. Furthermore, the first approach to the description of complex process data also includes the advanced interpretation of masterplot functions [41] (see Eqs. 4 and 5), which was recently found to provide valuable data in case of fully overlapping complex processes [34, 35, 41].

$$z(\alpha) = \Phi \cdot T^2 \tag{4}$$

$$y(\alpha) = \Phi \cdot e^{E/RT} \tag{5}$$

The second approach to description of complex kinetic data is based on mathematical deconvolution of the complex signal followed by single-process KA. In this approach certain appropriate mathematic function is used to separate the overlapping kinetic signals corresponding to the particular sub-processes. In this regard, the Fraser-Suzuki function (Eq. 6) was reported [9, 42] to reliably describe majority of solid-state kinetic processes, and it is nowadays used [43 - 45] as a standard choice for mathematic deconvolution. Note however, that the recent thorough testing [46] of the Fraser-Suzuki function has found certain limitations to its universality.

$$y = a_0 \exp\left[-\ln 2\left[\frac{\ln\left(1+2a_3\frac{x-a_1}{a_2}\right)}{a_3}\right]^2\right] \tag{6}$$

where a_0, a_1, a_2 and a_3 are the parameters corresponding to the amplitude, position, half-width and asymmetry of the peak, respectively.

The third approach to treating the complex kinetics is the kinetic deconvolution (sometimes denoted as formal KA), which utilizes non-linear optimization to simultaneously solve the full set of kinetic equations (similar to Eq. 1) corresponding to each involved sub-process. The present paper will utilize the multivariate kinetic analysis MKA [47] (Eqs. 7 and 8) as a main representative of this approach.

$$RSS = \sum_{j=1}^{n} \sum_{k=First_j}^{Last_j} w_j \left(Y\exp_{j,k} - Ycal_{j,k} \right)^2 \tag{7}$$

$$w_j = \frac{1}{\left| \left[d\alpha/dt \right]_{\max} \right|_j + \left| \left[d\alpha/dt \right]_{\min} \right|_j} \tag{8}$$

where *RSS* is the sum of squared residue, *n* is number of measurements, *j* is index of the given measurement, $First_j$ is the index of the first point of the given curve, $Last_j$ is the index of the last point of the given curve, $Yexp_{j,k}$ is the experimental value of the point *k* of curve *j*, $Ycal_{j,k}$ is the calculated value of the point *k* of curve *j* and w_j is weighting factor for curve *j*. Calculation of the theoretical data (Y_{cal}) is based on preselected kinetic mechanism reflecting the supposed interdependence of the involved kinetic sub-processes. In case of the present paper no interdependence between the crystallization sub-processes (corresponding to the crystal growth within each particular powder size fraction) was assumed. Note that, in general, the crystallization processes in glassy matrices are almost always independent. More so in the present case, when physical mixtures of the two solid phases with different kinetic characteristics were arbitrarily created. In such case the reaction model for Y_{cal} in MKA follows Eqs. 9 – 11.

$$d\alpha_1/dt = A_1 \cdot e^{-E_1/RT} \cdot f(\alpha_1) \tag{9}$$

$$d\alpha_2/dt = A_2 \cdot e^{-E_2/RT} \cdot f(\alpha_2) \tag{10}$$

$$\alpha = I_1\alpha_1 + I_2\alpha_2 \tag{11}$$

3. Experimental

The glassy selenium was prepared by melting the pure element (5N, Sigma-Aldrich) in an evacuated (to 10^{-5} Pa) fused silica ampoule at 450 °C for 20 h and letting the ampoule cool in air. The glassy ingot was then removed from the ampoule, ground in agate mortar and sieved through sieves with defined mesh to obtain the 20 – 50, 125 – 180 and 300 – 500 μm particle size fractions. Glassy nature of the prepared selenium material was checked by the Bruker AXS X-ray diffractometer D8 Advance equipped with a horizontal goniometer and scintillation counter utilizing CuK_{α} radiation. The check was performed on the finely ground powder fraction to confirm that the grinding itself did not cause degradation of the amorphous character – fully amorphous pattern with no diffraction lines was obtained.

The DSC measurements were performed by using the Q2000 (TA Instruments) heat-flow differential scanning calorimeter (DSC) with equipped T-zero technology and RCS90 cooling accessory. Six samples of each powder fraction with masses 10.0 ± 0.5 mg were hermetically sealed in aluminum pans and measured in the range of 10 – 250 °C at heating rates q^{+} = 0.5, 1, 2, 5, 10 and 20 °C·min^{-1}. In addition, similar sets of measurements were also performed for the combinations of the powder mixtures (20 – 50 + 300 – 500 μm; 125 – 180 + 300 – 500 μm; and 20 - 50 + 125 - 180 μm), where mass of each of the two respective powders put in the DSC pan was ~ 4 mg (track of the exact masses was kept for the consequent calculations; the mass-to-mass ratio was never diverged by more than 49/51 %). The DSC cell was purged with dry nitrogen at 30 cm^{3}·min^{-1}. Good reproducibility of the DSC data was checked by repeating two randomly selected measurements out of each dataset.

4. Results

In order to lay ground for the kinetic analysis of particle-size-based complex process scenarios, the single process kinetic analysis for the separate powder size fractions was

performed at first. Typical example of raw DSC curve measured for the 20 – 50 μm powder at 10 °C·min^{-1} is shown in Fig. 1A – characteristic features including the glass transition, crystallization and melting effects are apparent. The net crystallization signals were obtained by subtracting the thermokinetic background (DSC baseline). The calculation in terms of the physically meaningful tangential area-proportionate interpolation [48] (Eq. 12) was used to ensure maximum precision.

$$B(T) = (1 - \alpha(T)) \cdot (z_{0,r} + z_{1,r} \cdot T) + \alpha(T) \cdot (z_{0,p} + z_{1,p} \cdot (T_f - T)) \quad (12)$$

where $B(T)$ is the temperature dependence of the baseline curve, α is degree of conversion, $z_{0,r}$ and $z_{1,r}$ are the coefficients characterizing the tangent going through the starting point (in the reactants area), $z_{0,p}$ and $z_{1,p}$ are the coefficients characterizing the tangent going through the end point (in the products area) and T_f is the end point temperature. The net crystallization signals are for the separate powder fractions shown in Figs. 1B – 1D.

Single-process KA is methodologies-wise pretty straightforward [49] but a priori does not take into account the possible evolution of kinetic parameters (quantities from Eq. 1) with temperature – such as occurs [33 - 36] in case of Se glass crystallization. This issue has to be solved by and exploratory approach to both kinetic description and kinetic predictions. In Fig. 2 the main methodical solutions for evaluation of E are summarized. The simplest way, for the single-process data, is the application of the Kissinger equation [50] (Eq. 13):

$$\ln\left(\frac{q^+}{T_p^2}\right) = -\frac{E}{RT_p} + const. \quad (13)$$

where T_p is the temperature corresponding to the maximum of the DSC crystallization peak. As is apparent from Fig. 2A, the Kissinger plots are for all three separate powder fractions curved, which indicates continuous change of E with either T of q^+. Note that the essence of this behavior lies in the progressive transition between the two dominant crystal growth modes – each with significantly different activation energies [51 - 53]. Derivation of the

Kissinger dependences from Fig. 2A then gives the temperature dependence of E (for the maximum reaction rate) and shows good agreement of the E-T data between all three powder size fractions (see Fig. 2B), confirming the universal nature of this behavior with respect to the surface/volume ratio of the crystallizing particles. The apparently massive change of E with T is in correspondence with the previous studies on glassy Se. [33 - 36] Another standard approach used to determine E in case of simple processes are the isoconversional methods. The differential and integral E-α dependences are for the three separate powder fractions shown in Figs. 2C and 2D, respectively (note the recent review [8] on practical equality of all differential and integral isoconversional methods; Eqs. 2 and 3 were used in the present paper). In compliance with the general performance of these methods, the differential E-α dependence shows significantly higher scatter resulting from the punctual E values being determined based on both T_α and Φ_α. In comparison, the integral isoconversional methods show very clear trends in E with α and particle size. It should be, however, borne in mind that the isoconversional methods (expressed in this standard way) provide a potentially misleading view of the evaluated kinetics - the apparent evolution of E with α does not correspond to the variability of activation energy over the intrinsic course of the physical process but, instead, to the process kinetics changing with experimental conditions (evaluation of each point displayed in Figs. 2C and 2D is done by linearization of a dependence curved similarly to those shown in Fig. 2A). Also, due to the averaging of the activation energy over a wide temperature interval, the isoconversional methods do not correctly display the range of true E values driving the crystallization process during the non-isothermal heating.

Another very often used single-process KA methodology is the utilization and advanced interpretation of masterplot functions z(α) and y(α) [41] – see Eqs. 4 and 5. The masterplot functions are for the present data (the separated powder fractions) shown in Fig. 3. The highly consistent shapes of the masterplot functions indicate that the base reaction

mechanism f(α) does not change with T. Only in case of the coarse powders measured at high q^+ the masterplot shapes show moderate deviation from the prevailing course of the dependences due to the surface crystal growth increasing its manifestation at higher q^+. [33, 34] The z(α) maxima borderline correspond to the nucleation-growth kinetics ($\alpha_{max,z}$ = 0.63 [54]) but the flexible autocatalytic AC model [37] (Eq. 14) will be used for f(α) quantification instead. This will later help to comparatively account also for the complex kinetic behavior – the M and N terms are empirical dimensionless kinetic parameters.

$$f(\alpha) = \alpha^M (1-\alpha)^N \tag{14}$$

The AC model parameters M and N are for the separated Se powders shown in Fig. 4. Two evaluation methods were used – the double-logarithm method described e.g. in [37, 41] and the non-linear MKA optimization described by Eqs. 7 and 8. Whereas the MKA optimization evaluates (and averages) the overall shape of the kinetic peak, the double-logarithm method is primarily based on the value of the y(α) function maximum. The acceptable agreement between the results provided by the two methods corresponds to the manifestation of kinetic simplicity and almost ideally profiled kinetic peak. The unambiguously identifiable evolution of M and N with increasing temperature then reflects the progressing interchange between the volume and surface crystal growth mechanisms [33 – 36, 53].

As is apparent from the single-process KA applied to the crystallization data of the separated Se powder fractions, the kinetics is quite complicated, exhibiting temperature-dependent development of E (due to the switching growth modes [51 - 53]) and f(α) (due to the gradually changing ratio between the intensities of volume and surface crystallization manifestations. As was already mentioned in [32], such behavior can be considered ultimate kinetic complexity on its own. The issue can however become even more complicated when apparent (as-defined) kinetic complexity is introduced; i.e. overlap of several distinct kinetic

processes occurs. This case is in the present paper imitated by the overlaps of the crystallization signals corresponding to the particular Se powder size fractions – see the data in Fig. 5 (pure kinetic signals are being depicted, with the thermokinetic background already subtracted in correspondence with Eq. 12). The following section will discuss the performance of the particular complex-kinetics approaches to dealing with such type of complex data.

5. Discussion

The discussion over the performance of the particular KA approaches to complex kinetics will be conducted in three sections – one for each main type of approach as described in the theoretical part.

5.1. Approach No. 1: Single-process methods

Starting with the methods aimed at determination of E, the results of the Kissinger evaluation (Eq. 13) applied to complex kinetic crystallization data of mixed Se powder fractions (as depicted in Fig. 5) are shown in Fig. 6A. From the comparison with the data for the separate powders (red-based points in Fig. 6A) it is clear that the apparent overall maximum transformation rate is shifted to slightly higher temperature with the addition of coarser powder fraction but the dominant signal always comes from the finest fraction of the mixture. This behavior can be explained by a combination of two consequences of the self-heating effect [55]. Firstly, the finer (more reactive) powder fraction is “diluted” by the presence of coarser grains, which slows down the average reaction rate and hence shifts the signal to slightly higher temperature. The physical basis for this effect lies in the lower local overheating effect (due to the self-heating mechanism characteristic for the exothermic processes, such as the crystallization). The second effect is that of the surface overheating

(with respect to the average temperature in the DSC cell) of the coarse powder grains, which evidently initiates and also markedly accelerates the crystal growth throughout the glassy matrix. This is evidenced by the data in Fig. 6A corresponding to the mixture of the 125 – 180 + 300 – 500 μm powder fractions. Note that powdered glassy selenium preferentially crystallizes from surface [33 – 36] and even the bulk Se samples with very low amount of mechanically induced defects [31] exhibit non-negligible amount of surface crystallinity [53].

Nevertheless, despite the significant temperature shifts of the kinetic peaks corresponding to the mixtures of powders, the resulting activation energies derived from the Kissinger plot (and expressed as a temperature dependence) are practically not influenced – see Fig. 6B where the lines correspond to the data obtained for the separated powder fractions from Fig. 2B. It has to be however noted that these data reflect only the dominant (or the effectively dominant) kinetic process. This robustness in relation to the kinetic complexity is the main advantage of the Kissinger (or any other T_p-based) evaluation method as was already reported in [56]. Similar comparison is in Figs. 6C and 6D shown for the isoconversional methods. The differential Friedman method in Fig. 6C (with the lines corresponding to the data from Fig. 2C) and the integral Starink method in Fig. 6D (with the lines corresponding to the data from Fig. 2D). In general, the full overlaps of sub-processes with close activation energies are difficult to recognize and interpret via the isoconversional methods [38, 56]. This is indeed also the case of the present data, where the kinetic complexity would be uneasy to recognize without the knowledge/comparison with the data for the separated Se powders. However, the data corresponding to the mixtures of closely sized Se powder fractions (20 – 50 + 125 – 180 μm, and 125 – 180 + 300 – 500 μm) can be associated with the very question of the definition of kinetic complexity itself, which will be discussed in the concluding section of this paper. Regarding the mixture of well-separated powder fraction sizes (20 – 50 + 300 – 500 μm), it is interesting that even in such case of evidently complex transformation

mechanism with significantly different E values associated with each sub-process the integral isoconversional method (Fig. 6D) shows a gradually changing E-α dependence, qualitatively similar to those of separated Se powders. The differential isoconversional method, on the contrary, unambiguously shows a step-like decrease of E, corresponding to the switch between the dominating contributions from the particular sub-processes.

Apart from the isoconversional methods, also the masterplot (Eqs. 4 and 5) interpretation [41] can be sometimes used to reveal additional information about the complex processes – especially in case of the fully overlapping processes. The masterplot analysis, i.e. the z(α) and y(α) functions, is for the mixtures of Se powders shown in Fig. 7. Mixtures of the closely sized Se powder fractions (Figs. 7A – 7D) exhibit uniform round shape of the masterplots (without any shoulders) and also the position of the maxima does not change with q^+. These characteristics indicate that the kinetics of both sub-processes are very similar, which is indeed evidenced by the lines corresponding to the masterplot functions obtained for the two respective separated powder fractions at 5 °C·min^{-1} (note that when forced the physically meaningful nucleation-growth [57 - 60] description, all separated Se powder fractions exhibited results corresponding to the dominant surface crystallization). Moreover, note the shift of the masterplot maxima of powders mixtures to lower α values for the future reference in the concluding section. The mixture of the well-separated powders (Figs. 7E and 7F) then shows the typical double-peak shape; the evolution in magnitude of the high-α shoulder corresponds to the documented [33 – 36] change of the crystal growth mechanics in case of very coarse powders (at higher q^+ the occurrence of volume-located crystallites recedes at the expense of the surface crystalline layer thickness).

5.2. Approach No. 2: Mathematic deconvolution

As adverted in the theoretical section, the mathematic deconvolution was performed by using the Fraser-Suzuki function (Eq. 6). Considering the meaning of the Fraser-Suzuki parameters, it is only the asymmetry parameter a_3 that can be used to characterize certain kinetic behavior. In order to utilize this possibility, the kinetic data obtained for the separated powder fractions (see Fig. 1) were fitted by the Fraser-Suzuki function. The obtained asymmetry parameters a_3 are listed in Table 1. Consequently, two variations of the Fraser-Suzuki deconvolution were applied to the complex kinetic data corresponding to the powder mixtures (see Fig. 5): in the first batch the data were deconvoluted without any restrictions (i.e. with all parameters allowed for optimization), and in the second batch the a_3 parameters were set fixed for each respective combination of q^+ and powder size in the mixture in accordance with the data from Table 1. Each batch of deconvoluted data was then evaluated by means of single-process KA in terms of the AC model, i.e. using the averaged Kissinger fit, double logarithm determination of M and N kinetic exponents, determination of the masterplot maxima, and determination of A via the non-linear optimization (utilizing the previously obtained E, M and N).

The results of single-process KA following the two batches of Fraser-Suzuki deconvolution are for the 20 – 50 + 300 – 500 μm mixture compared with the description obtained for the separated powders in Tables 2 and 3. At first sight, it seems that a reasonable agreement was achieved for both types/batches of the deconvolution, with slightly better results provided for the parameter a_3 being fixed to correct value. However, the I_1/I_2 ratio was found to be determined significantly incorrectly (note that the masses of each powder in each mixture and during each DSC measurement were accurately weighted) in both deconvolution batches. The results are compared to the correct values in Fig. 8. Better agreement between the correct (physically input) and determined (from the deconvolution) I_1/I_2 values was achieved only after iterative process of fixing the Fraser-Suzuki parameter a_0 (corresponding

to the peak height) at arbitrarily chosen values. Even greater difficulties were encountered when the mixtures of closely sized Se powder fractions (20 – 50 + 125 – 180 μm, and 125 – 180 + 300 – 500 μm) were deconvoluted. In this case the optimization algorithm usually preferred combination of one negatively and one positively asymmetric peak, and only several rounds of iterative operations (utilizing fixation of certain Fraser-Suzuki parameters) led to a reasonable description of the involved crystallization sub-processes qualitatively comparable to that reported in [34].

5.3. Approach No. 3: Kinetic deconvolution

The third approach applied to determine detailed kinetics of the Se powders mixtures was based on the multivariate kinetic analysis (Eqs. 7 – 11). Unlike mathematic deconvolution, the MKA treatment can be utilize the results of model-free KA (i.e. independent determination of E and A) to improve the optimization procedure. Kinetic deconvolution has thus large variety of options for adjusting the kinetic results based on the information provided not only by complementary thermo-analytic techniques (observing the process via evolution of various physico-chemical properties/quantities) but also by the adjacent KA methods focusing on the determination of the kinetic parameters in different ways (sometimes revealing behavioral relations and connections that MKA cannot recognize).

The different approaches will first be tested on the rather unambiguously resolved 20 – 50 + 300 – 500 μm mixture dataset (see Fig. 5C); for simplicity the parameters corresponding to the first appearing process (crystallization of the 20 – 50 μm powder within the mixture) will be indexed “1” and the second process (crystallization of the 300 – 500 μm powder) will be indexed “2”. The base and simplest procedure to the kinetic deconvolution is to fit the whole set of Eqs. 7 – 11 simultaneously for all data-curves and without any restrictions. Such approach resulted in the following set of kinetic parameters: $E_1 = 102.0\ kJ \cdot mol^{-1}$,

E_2 = 93.4 kJ·mol^{-1}, M_1 = 0.67, N_1 = 1.44, M_2 = 0.77, N_2 = 1.12, I_1/I = 0.74, logA_1 = 12.73, logA_2 = 11.22. In comparison with the single-process KA applied to the two corresponding separated Se powders (see Tables 2 and 3; the average I_1/I was 0.494), the simultaneous optimization of all kinetic curves gives exceptionally inaccurate results, which is the consequence of the simultaneous MKA trying to average both, the temperature dependent model-free and model-based components of the Se mixture crystallization kinetics. In order to improve the results, single-curve MKA [32] can be applied, which optimizes each data-curve separately with E being fixed (i.e. set constant at a selected value). In Fig. 9 three batches of optimizations performed for the data corresponding to the 20 – 50 + 300 – 500 μm mixture are compared with the single-curve MKA results obtained for the separated 20 – 50 μm and 300 – 500 μm Se powders: the first batch of mixture kinetic optimization was performed for the activation energies fixed at values obtained from the overall simultaneous optimization (E_1 = 102.0 kJ·mol^{-1} and E_2 = 93.4 kJ·mol^{-1}), the second batch of optimizations was done for the same E values and correct I_1/I_2 ratios (depicted in Fig. 8), and the third batch of optimizations was done for the E values obtained from the Kissinger evaluation (E_1 = 117.7 kJ·mol^{-1} and E_2 = 106.4 kJ·mol^{-1}) and again with fixed correct I_1/I_2 ratios. As expected, the utilization of the single-curve MKA alone dramatically improved the accuracy of the determination of the AC kinetic exponents. The second most important factor was the implemented knowledge of the ratio between the two involved processes I_1/I_2. Lastly, regarding the different used E values, Fig. 9 shows that the usage of activation energies provided by the Kissinger equation resulted in moderately better estimation of M and N exponents. This is however a consequence of the same E values having been used also during the single-curve MKA evaluation of the separated powders kinetics. If the E values obtained from the overall simultaneous optimization (E_1 = 102.0 kJ·mol^{-1} and E_2 = 93.4 kJ·mol^{-1}) are used for the fit of the separated powders data, then the red points in Fig. 9 shift significantly

(see the Supplemental online material) and the overall comparison ends up only very slightly in favor of the E values provided by the Kissinger equation. In conclusion, the method of E determination is largely irrelevant under the assumption that the same approach/data is used also in the akin (potentially comparable) evaluations and in the consequent predictions of the kinetic behavior.

Similar analysis was performed also for the fully overlapping combinations of the sub-processes, i.e. 20 – 50 + 125 – 180 µm, and 125 – 180 + 300 – 500 µm powder mixtures. Optimization without any restrictions resulted in very skewed results: for the 20 – 50 + 125 – 180 µm mixture the kinetic parameters were E_1 = 157.6 kJ·mol^{-1}, E_2 = 96.6 kJ·mol^{-1}, M_1 = 0.53, N_1 = 0.81, M_2 = 0.71, N_2 = 1.19, I_1/I = 0.11, logA_1 = 20.63, logA_2 = 11.97, and for the 125 – 180 + 300 – 500 µm mixture the kinetic parameters were E_1 = 139.6 kJ·mol^{-1}, E_2 = 90.8 kJ·mol^{-1}, M_1 = 0.45, N_1 = 0.83, M_2 = 0.69, N_2 = 1.24, I_1/I = 0.21, logA_1 = 17.70, logA_2 = 10.92. Consequently, the single-curve MKA was performed in two variations/batches. First batch of MKA optimizations was done only with the E values fixed – the activation energies determined via the Kissinger equation were taken. Note that it was shown in the previous paragraph for the 20 – 50 + 300 – 500 µm mixture that the choice of the model-free methodology has only minor impact on the single-curve MKA kinetic deconvolution. In the second batch of optimization both, the E and I_1/I values were fixed at correct values. As is shown in Fig. 10, surprisingly good agreement between the AC kinetic exponents determined from the separated powders data and from the MKA-deconvoluted mixtures with fully overlapping crystallization peaks was obtained. Fixation of the I_1/I term at correct value during the non-linear optimization brought however only very marginal improvement of the results. The kinetic deconvolution was hereby shown to be able to provide relevant and quite accurate information about the kinetic sub-processes even in case of their full overlap.

5.4. Additivity of the crystallization signals

Performance of the three most important approaches to kinetic analysis of complex processes was examined for three cases of arbitrarily created mixtures of selenium powders with different grain size. So far, the additivity of the kinetic signals of the separated Se powders was assumed in the evaluations (and hence the kinetic parameters obtained for the separated powders were presented as the true values in all comparisons). In order to verify this assumption, the signals corresponding to the three experimentally measured powder mixtures were theoretically modeled based on the kinetic parameters of the separated powders (with all individual descriptions having r^2 over 0.9999 during the single-curve MKA) and the true I_1/I_2 (masses weighted into the DSC pans). This comparison is demonstrated in Fig. 11 for the data-curves obtained at $q^+ = 5\ °C \cdot min^{-1}$. Points indicate the experimental data for the respective mixtures and the dashed line shows the simulated "prediction" based on the data from separated powders - the agreement is evidently poor. However, only by adjusting of the position of the kinetic peaks on the temperature axis (i.e. by slightly changing the pre-exponential factors A_1 and A_2, which was done by fitting each experimental data by the AC kinetics corresponding to the two respective separated powders with only $\log A_1$ and $\log A_2$ being allowed to optimize) an exceptionally good agreement was obtained. Identical behavior and conclusions were obtained also for all other data-curves obtained at different q^+.

This finding verifies the foundation (base assumption) of the performance evaluations discussed in the present paper. The crystallization signals are perfectly additive (if accounting for a slight delay, which will be discussed momentarily) with respect to the activation energies, AC kinetic exponents and I_1/I_2 ratio. In other words, these kinetic quantities are not affected by additive mixing of the crystallizing powders. Hence, during the reverse procedure, i.e. the complex-process kinetic analysis, it is legitimate to require precise determination of E, M, N and I_1/I values for each crystallization sub-process.

The same pattern of the temperature shift, such as depicted in Fig. 11, was identified for all data-curves (measured at different q^+) of all three Se powder mixtures. This indicates that there is an underlying physical cause for the crystallization of mixed powders being shifted to slightly higher temperature. Closer examination reveals that it is always the crystal growth in the finer powder that gets hindered; crystallization of the coarser powder remains practically unchanged. This phenomenon corresponds to the effect of self-heating, where the heat released during the amorphous-to-crystalline transformation causes local increase of temperature and, consequently, autocatalytically accelerates further crystal growth. In case of the present data, the finer powder gets diluted by the coarser one (which at the initial stage acts practically as an inert compound because its crystallization starts later due to the lower amount of mechanically induced defects [31]), the amount of initially evolved heat is lower and the autocatalytic overheating effect cumulates more slowly. Hence the shift of the crystallization data to higher temperature. The resistance of the coarser powders to this autocatalytic overheating effect can then be explained based on the significantly lower amount of mechanical defects being present. It is very probably these nucleation/growth active centers that initiate the crystallization and rapidly react to the first increase of temperature (be it only during local overheating). Lack of these active centers then decreases the influence of local temperature fluctuations. This concept is supported by the data in Figs. 11A and 11B, where the difference between the simulated and experimental data is evidently larger for the set of finer powders (graph A).

6. Conclusions

Performance of the methods of kinetic analysis appropriate for evaluation of the complex kinetic data was determined for the arbitrarily created complexity based on the simultaneous crystallization of selenium powders with different particle sizes (and different

reactivity). Scenarios with both, partial and full overlaps of the transformation mechanisms were created. Accuracy of the tested methods was considered based on the comparison with the single-process evaluations performed for each separate powder fraction; additivity of the data was verified by an independent fit with included discussion over the influence of the self-heating effect in case of exothermic processes.

Interpretation of single-process KA methods focused on determination of E resulted in acceptable conclusions – the T_p-based methods (e.g. Kissinger equation) and differential isoconversional methods performed very well in case of the partial overlaps, where the true activation energies of the involved sub-processes were obtained. The integral isoconversional methods, on the other hand, averaged the E values not only for the fully overlapping kinetic peaks but also for the partial overlap, without real possibility to even recognize the kinetic complexity. Crucial information about the temperature evolution of the overall crystallization kinetics was provided by the E-T dependence derived from the Kissinger plot. Regarding the masterplot analysis, this methodology should be in practice considered only for revelation of the possible partial kinetic overlaps. Masterplot functions are very sensitive to the presence of shoulders and minor sub-peaks in the kinetic data, as indicated by the shift of the masterplot maxima even for the full overlaps (see Fig. 7).

Mathematic deconvolution followed by the single-process KA worked reasonably well in case of the partially overlapping processes. Acceptably precise values of E, A, M and N were obtained during the zeroth iteration of non-linear optimization even without any parameter of Fraser-Suzuki function being restricted. Restriction of the peak asymmetry then brought only marginal improvement. However, the ratio between the magnitudes of the involved sub-processes I_1/I_2 was determined very inaccurately and its improvement would require series of subjective iterative corrections. In case of the fully overlapping kinetic peaks the non-restricted mathematic deconvolution provided completely incorrect results and

additional information about the nature of the sub-processes (e.g. possible kinetic models to adjust asymmetry, intensities of manifestation to set I_1/I_2) would be mandatory to obtain meaningful results.

In case of the kinetic deconvolution the only real option was to use the single-curve MKA due to the significant trends in crystallization kinetics with increasing temperature [32]. This method worked well for both, partially and fully overlapping kinetic data. Implementation of the correct I_1/I_2 led to only slight improvement of the results; evaluation method for the fixed E values practically did not matter.

To conclude, in complex scenarios with significant or full kinetic overlaps the best option is to use the single-curve kinetic deconvolution with the activation energy values being provided either by the T_p-based methods or the differential isoconversional methods. Alternatively, mathematic deconvolution utilizing the Fraser-Suzuki function can be used; however it is paramount to combine this approach with additional sources of information about the physical nature and intensity of manifestation of the involved sub-processes (e.g. temperature-resolved XRD, thermogravimetry, temperature-resolved Raman spectroscopy, microscopy, etc.).

As a finishing remark, it can be stated that the particle-size resolved studies are very important for understanding the trends in kinetic behavior of most solid-state materials. However, increased attention should be paid to the fact that the segregation of the particle size powder fractions is done arbitrarily and as such should be performed with respect to the relevant practical applications considered for the given material. Division of the particular powder fractions should be sufficiently narrow to reflect the specific behavioral features of the given grain sizes, with the scale refinement borderline being the constancy/plateau reached in the values of determined kinetic parameters. Very important aspect of such studies is the verification of additivity of the kinetic data.

Acknowledgments

This work has been supported by the Czech Science Foundation under project No. 17-11753S.

References

[1] J. Cai, W. Wu, R. Liu. Isoconversional Kinetic Analysis of Complex Solid-State Processes: Parallel and Successive Reactions. Ind. Eng. Chem. Res. 51 (2012) 16157-16161.

[2] N. Sbirrazuoli, Y. Girault, L. Elegant. Simulations for evaluation of kinetic methods in differential scanning calorimetry. Part 3. Thermochim. Acta 293 (1997) 25-37.

[3] N.I. Vaganova, V.I. Rozenband, V.V. Barzykin. Application of thermal analysis to the study of the kinetics of 2-stage reactions. J. Therm. Anal. 34 (1988) 71-83.

[4] J.M. Criado, M. Gonzalez, A. Ortega, C. Real. Discrimination of the kinetic model of overlapping solid-state reactions from non-isothermal data. J. Therm. Anal. 34 (1988) 1387.

[5] N.I. Vaganova, V.I. Rozenband, V.V. Barzykin. Thermoanalytical studies of the kinetic of reversible reactions. J. Therm. Anal. 34 (1988) 949-962.

[6] S.V. Vyazovkin, A.I. Lesnikovich. An approach to the solution of the inverse kinetic problem in the case of complex processes 1. Thermochim. Acta 165 (1990) 273-280.

[7] J.M. Criado, P.E. Sanchez-Jimenez, L.A. Perez-Maqueda. Critical study of the isoconversional methods of kinetic analysis. J. Therm. Anal. Calorim. 92 (2008) 199−203.

[8] J.M. Cai, S.Y. Chen. A new iterative linear integral isoconversional method for the determination of the activation energy varying with the conversion degree. J. Comput. Chem. 30 (2009) 1986−1991.

[9] A. Perejon, P.E. Sanchez-Jimenez, J.M. Criado, L.A. Perez-Maqueda. Kinetic analysis of complex solid-state reactions. A new deconvolution procedure. J. Phys. Chem. B 115 (2011) 1780−1791.

[10] S.V. Golikeri, D. Luss. Analysis of activation energy of grouped parallel reactions. AIChE J. 18 (1972) 277-282.

[11] R. Svoboda. Tangential area-proportional baseline interpolation for complex-process DSC data – yes or no? Thermochim. Acta 658 (2017) 55-62.

[12] R. Svoboda. Importance of proper baseline identification for the subsequent kinetic analysis of derivative kinetic data, part 3. J. Therm. Anal. Calorim. 136 (2019) 1307-1314

[13] L. Nowicki, D. Siuta, M. Godala. Determination of the chemical reaction kinetics using isothermal reaction calorimetry supported by measurements of the gas production rate: A case study on the decomposition of formic acid in the heterogeneous Fenton reaction. Thermochimica Acta 653 (2017) 62-70.

[14] N.V. Muravyev, A.N. Pivkina. New concept of thermokinetic analysis with artificial neural networks. Thermochimica Acta 637 (2016) 69-73.

[15] M. Catauro, A. Dell'Era, S.V. Ciprioti. Synthesis, structural, spectroscopic and thermoanalytical study of sol-gel derived SiO2-CaO-P2O5 gel and ceramic materials. Thermochimica Acta 625 (2016) 20-27.

[16] S. Zeman, Q.L. Yan, M. Gozin, F.Q. Zhao, Z. Akstein. Thermal behavior of 1,3,5-trinitroso-1,3,5-triazinane and its melt-castable mixtures with cyclic nitramines. Therochimica Acta 615 (2015) 51-60.
[17] M. Khachani, A. El Hamidi, M. Kacimi, M. Halim, S. Arsalane. Kinetic approach of multi-step thermal decomposition processes of iron(III) phosphate dihydrate FePO4 center dot 2H(2)O. Thermochimica Acta 610 (2015) 29-36.
[18] E.J. Grajales, E.A. Alacron, A.L. Villa. Kinetics of depolymerization of paraformaldehyde obtained by thermogravimetric analysis. Thermochim. Acta 609 (2015) 49-60.
[19] N.N. Begovic, N.N. Stojanovic, S.B. Ostojic, A.M. Radulovic, V.A. Blagojevic, B. Simonovic, D.M. Minic. Thermally induced polymerization of binuclear [Ni-2(en)(2)(H2O)(6)(pyr)]center dot 4H(2)O complex. Thermochim. Acta 607 (2015) 82-91.
[20] R. Font. Potential kinetic model for thermal decomposition of complex organic compounds: Significance of parameters and engineering application. Thermochimica Acta 591 (2014) 81-95.
[21] R. Svoboda, J. Málek. Extended study of crystallization kinetics for Se-Te glasses. J. Therm. Anal. Cal. 111 (2013) 161-171
[22] R. Svoboda, J. Málek. Thermal behavior in Se-Te chalcogenide system: Interplay of thermodynamics and kinetics. J. Chem. Phys. 141 (2014) 224507
[23] R. Svoboda, J. Málek. Thermal behavior of Se-rich $Ge_2Sb_2Se_{(5-y)}Te_y$ chalcogenide system. J. Alloys Compd. 627 (2015) 287-298
[24] R. Svoboda, J. Málek. Particle size dependent isothermal crystallization kinetics in a Se-Te glassy system. Thermochimica Acta 610 (2015) 47-56
[25] R. Svoboda. Oxidation-influenced crystallization in $(GeSe)_x(Sb_2Se_3)_{1-x}$ chalcogenide glasses. J. Non-Cryst. Sol. 510 (2019) 6-14
[26] R. Svoboda, J. Málek. Thermal behavior of Se-rich $GeSb_2Se_{(4-y)}Te_y$ (glassy) system. J. Alloys Compd. 670 (2016) 222-228
[27] R. Svoboda, D. Brandová, J. Málek. Thermal behavior of $Ge_{20}Se_yTe_{80-y}$ infrared glasses (for *y* up to 8 at.%). J. Alloys Compd. 680 (2016) 427-435
[28] R. Svoboda. Oxidation-accelerated crystallization of $(GeS_2)_y(Sb_2S_3)_{1-y}$ chalcogenide glasses. J. Non-Cryst. Sol. 456 (2017) 88-94
[29] R. Svoboda, D. Brandová. Crystallization behavior of $(GeTe_4)_x(GaTe_3)_{100-x}$ glasses for far-infrared optics applications. J. Alloys. Compd. 770 (2019) 564-571
[30] D. Brandová, R. Svoboda. Themo-structural characterization of $(As_2Se_3)_{100-x}$-$(As_2Te_3)_x$ glasses for far-infrared optics. J. Am. Ceram. Soc. 102 (2019) 382-396
[31] R. Svoboda, D. Brandová. Crystal growth from mechanically induced defects: A phenomenon observed for glassy materials. J. Therm. Anal. Calorim. 127 (2017) 799 - 808
[32] D. Brandová, R. Svoboda, Z. Olmrová Zmrhalová, J. Chovanec, R. Bulánek. Crystallization kinetics of glassy materials: the ultimate complexity? J. Therm. Anal. Calorim. 134 (2018) 825-834.
[33] R. Svoboda, J. Málek. Crystallization kinetics of a-Se, part 1: Interpretation of kinetic functions. J. Therm. Anal. Cal. 114 (2013) 473-482
[34] R. Svoboda, J. Málek. Crystallization kinetics of a-Se, part 2: Deconvolution of a complex process – the final answer. J. Therm. Anal. Cal. 115 (2014) 81-91
[35] R. Svoboda, J. Málek. Crystallization kinetics of a-Se, part 3: Isothermal data. J. Therm. Anal. Calorim. 119 (2015) 1363-1372
[36] R. Svoboda, J. Gutwirth, J. Málek. Crystallization kinetics of a-Se, part 4: Thin films. Phil. Mag. 94 (2014) 3036-3051.

[37] J. Šesták. Thermophysical Properties of Solids, Their Measurements and Theoretical Analysis. Elsevier: Amsterdam, 1984.
[38] G. Luciano, R. Svoboda. Activation energy determination in case of independent complex kinetic processes. Processes 7 (2019) 738
[39] H.L. Friedman, Kinetics of thermal degradation of char-forming plastics from thermogravimetry. Application to a phenolic plastic, J. Polym. Sci., Part C 6 (1964) 183–195
[40] M.J. Starink. The determination of activation energy from linear heating rate experiments: a comparison of the accuracy of isoconversion methods, Thermochim. Acta 404 (2003) 163–176
[41] R. Svoboda, J. Málek. Interpretation of crystallization kinetics results provided by DSC. Thermochimica Acta 526 (2011) 237-251
[42] R. Svoboda, J. Málek. Applicability of Fraser-Suzuki function in kinetic analysis of complex processes. J. Therm. Anal. Cal. 111 (2013) 1045-1056.
[43] N. Manic, B. Jankovic, V. Dodevski, D. Stojiljkovic, V. Jovanovic. The Pyrolysis of Waste Biomass Investigated by Simultaneous TGA-DTA-MS Measurements and Kinetic Modeling with Deconvolution Functions. Lecture Notes in Networks and Systems 90 (2020) 39-60.
[44] X. Yao, L. Ni, J. Jiang, J. Huang, J. Yang, G. Yang. Thermal hazard and kinetic study of 5-(2-pyrimidyl) tetrazole based on deconvolution procedure. J. Loss Prevent. Proc. 61 (2019) 58-65.
[45] P. Stolarek, S. Ledakowitz, R. Slezak. Influence of Liming on Kinetics of Sewage Sludge Pyrolysis. Ecol. Chem. Eng. S 26 (2019) 175-188.
[46] R. Svoboda. Fraser-Suzuki function in kinetic analysis of complex solid-state reactions. Phys. Chem. Chem. Phys. – submitted.
[47] J. Opfermann. Kinetic analysis using multivariate non-linear regression. I. basic concepts. J. Therm. Anal. Calorim. 60 (2000) 641-658.
[48] J. Šesták. Science of Heat and Thermophysical Studies: A Generalized Approach to Thermal Analysis, Elsevier, Amsterdam, 2005.
[49] S. Vyazovkin, A.K. Burnham, J.M. Criado, L.A. Pérez-Maqueda, C. Popescu, N. Sbirrazzuoli, ICTAC Kinetics Committee recommendations for performing kinetic computations on thermal analysis data, Thermochim Acta. 520 (2011) 1–19.
[50] H.E. Kissinger, Reaction kinetics in differential thermal analysis, Anal.Chem. 29 (1957) 1702-1706
[51] G. Ryschenkow, G. Faivre. Bulk crystallization of liquid selenium. J. Cryst. Growth 87 (1988) 221-35.
[52] J. Bisault, G. Ryschenkow, G. Faivre. Spherulitic branching in the crystallization of liquid selenium. J. Cryst. Growth 110 (1991) 889-909.
[53] J. Málek, R. Svoboda. Kinetic processes in amorphous materials revealed by thermal analysis: Application to glassy selenium. Molecules 24 (2019) 2725
[54] J. Malek, The kinetic-analysis of nonisothermal data, Thermochim. Acta 200 (1992) 257–269.
[55] B. Lvov, V.L. Ugolkov. The self-heating effect in the process of $KMnO_4$ decomposition in vacuum. J. Therm. Anal. Calorim. 94 (2008) 453-460.
[56] R. Svoboda, J. Málek. Is the original Kissinger equation obsolete today? J. Therm. Anal. Calorim. 115 (2014) 1961-1967
[57] W.A. Johnson, K.F. Mehl. Reaction kinetics in processes of nucleation and growth. Trans. Am. Inst. Min. (Metall) Eng. 135 (1939) 416–42.
[58] M. Avrami. Kinetics of phase change I–general theory. J. Chem. Phys. 7 (1939) 1103–12.

[59] M. Avrami. Kinetics of phase change. II–transformation-time relations for random distribution of nuclei. J. Chem. Phys. 7 (1940) 212–24.
[60] M. Avrami. Granulation, phase change, and microstructure – kinetics of phase change III. J. Chem. Phys. 7 (1941) 177–84.

Table 1
Fraser-Suzuki asymmetry parameter for separate 20 – 50 µm and 300 – 500 µm kinetic data-peaks.

q^+ / °C·min^{-1}	0.5	1	2	5	10	20
a_3 for 20 – 50 µm	-0.1691	-0.1655	-0.1366	-0.2054	-0.2222	-0.1735
a_3 for 300 – 500 µm	-0.2307	-0.2248	-0.1951	-0.2498	-0.1779	-0.1221

Table 2
Results of single process KA applied to separate 20 – 50 µm Se powder (denoted "20-50"), data corresponding to the 20 – 50 + 300 – 500 µm mixture deconvoluted using the Fraser-Suzuki function without any restrictions (denoted 20-50*), and the data of the 20 – 50 + 300 – 500 µm mixture treated by the Fraser-Suzuki deconvolution with parameter a_3 set fixed according Table 1(denoted 20-50**).

size / µm	20–50	20–50*	20–50**
E / kJ·mol^{-1}	117.7 ± 4.9	118.3 ± 5.2	118.3 ± 5.2
log(A/s^{-1})	15.04 ± 0.03	14.98 ± 0.19	14.96 ± 0.27
$\alpha_{max,z}$	0.587 ± 0.022	0.562 ± 0.031	0.559 ± 0.018
$\alpha_{max,y}$	0.419 ± 0.017	0.386 ± 0.047	0.395 ± 0.040
M	0.70 ± 0.10	0.57 ± 0.12	0.60 ± 0.13
N	0.96 ± 0.09	0.90 ± 0.05	0.90 ± 0.06

Table 3
Results of single process KA applied to separate 300 – 500 µm Se powder (denoted "300-500"), data corresponding to the 20 – 50 + 300 – 500 µm mixture deconvoluted using the Fraser-Suzuki function without any restrictions (denoted 300-500*), and the data of the 20 – 50 + 300 – 500 µm mixture treated by the Fraser-Suzuki deconvolution with parameter a_3 set fixed according Table 1(denoted 300-500**).

size / µm	300–500	300–500*	300–500**
E / kJ·mol^{-1}	106.4 ± 5.0	106.4 ± 5.0	106.4 ± 5.0
log(A/s^{-1})	12.84 ± 0.10	12.82 ± 0.06	12.83 ± 0.08
$\alpha_{max,z}$	0.596 ± 0.019	0.502 ± 0.049	0.573 ± 0.019
$\alpha_{max,y}$	0.373 ± 0.056	0.362 ± 0.036	0.366 ± 0.047
M	0.55 ± 0.11	0.51 ± 0.07	0.52 ± 0.08
N	0.91 ± 0.06	0.89 ± 0.09	0.89 ± 0.05

Figure captions

Fig. 1: A) Example DSC curve measured for the 20 – 50 μm powder at 10 °C·min^{-1}.
B) Set of DSC crystallization curves obtained at different heating rates for the 20 – 50 μm Se powder.
C) Set of DSC crystallization curves obtained at different heating rates for the 125 – 180 μm Se powder.
D) Set of DSC crystallization curves obtained at different heating rates for the 300 – 500 μm Se powder.

Fig. 2: A) Kissinger plot for the three discrete Se powders.
B) Temperature dependence of activation energy obtained from the derivative Kissinger plot for the three discrete Se powders.
C) Activation energy obtained by Friedman method for the three discrete Se powders.
D) Activation energy obtained by Starink method for the three discrete Se powders.

Fig. 3: Masterplot functions z(α) and y(α) for the three discrete Se powders.

Fig. 4: Kinetic exponents M and N of the AC model determined by single-curve MKA (red-based points in the graphs) and by the double-logarithm method (black-based points in the graphs) for the three discrete Se powders. Graphs A, B and C depict data for the 20 – 50, 125 – 180 and 300 – 500 μm particle size fractions, respectively.

Fig. 5: A) Set of DSC crystallization curves obtained at different heating rates for the mixture of 20 – 50 μm + 125 – 180 μm Se powders.
B) Set of DSC crystallization curves obtained at different heating rates for the mixture of 125 – 180 μm + 300 – 500 μm Se powders.
C) Set of DSC crystallization curves obtained at different heating rates for the mixture of 20 – 50 μm + 300 – 500 μm Se powders.

Fig. 6: A) Kissinger plot comparing the data for mixtures of Se powders (black-based data) and the three discrete Se powders (red-based data).
B) Temperature dependence of activation energy obtained from the derivative Kissinger plot for the three mixtures of Se powders. Lines correspond to the data for discrete Se powders from Fig. 2B.
C) Activation energy obtained by Friedman method for the three mixtures of Se powders. Lines correspond to the data for discrete Se powders from Fig. 2C.
D) Activation energy obtained by Starink method for the three mixtures of Se powders. Lines correspond to the data for discrete Se powders from Fig. 2D.

Fig. 7: Masterplot functions z(α) and y(α) for the three mixtures of Se powders. Lines depict the corresponding masterplot functions obtained for the 5 °C·min^{-1} data of the two discrete Se powders involved in the given mixture.

Fig. 8: Comparison of the I_1/I terms obtained during the unrestricted and restricted (fixed a_3 parameter) Fraser-Suzuki deconvolution of the 20 – 50 μm + 300 – 500 μm powders mixture with the true values calculated based on the masses of powders introduced into the DSC pans.

Fig. 9: Kinetic exponents M and N of the AC model determined by single-curve MKA applied to the mixture of 20 – 50 µm + 300 – 500 µm powders (black-based points) compared with the similarly obtained M and N values for the respective discrete powers (red based points). Three series of MKA optimization were performed – free optimization (white points), optimization with fixed I_1/I_2 (grey points), and optimization with fixed I_1/I_2 and E equal to that determined via Kissinger equation (black points).

Fig. 10: Kinetic exponents M and N of the AC model determined by single-curve MKA applied to the mixture of 20 – 50 µm + 125 – 180 µm powders (graphs A - D) and mixture of 125 – 180 µm + 300 – 500 µm powders (graphs E - F). Each graph shows comparison of the data obtained for the respective discrete powers (red based points) and two values obtained for the given mixture - free optimization (white points), optimization with fixed I_1/I_2 (grey points). Particle size legends in each graph correspond to the given mixture, where the bold letters standing outside of the parentheses denote the particular deconvoluted peak for which the evaluation is depicted.

Fig. 11: Comparison of the experimental crystallization data obtained at 5 °C·min^{-1} for the three mixtures (points) and the corresponding simulated signal obtained by summing the two signals of the two corresponding discrete powders (also obtained at 5 °C·min^{-1}) in the correct I_1/I_2 ratio used for the given mixture measurement (dashed lines). Red solid lines indicate fit of the experimental mixtures data by the two (previously only summed) signals corresponding to the two involved discrete powders with only their position (pre-exponential factor A) allowed for optimization.

Figure 1

Click here to download high resolution image

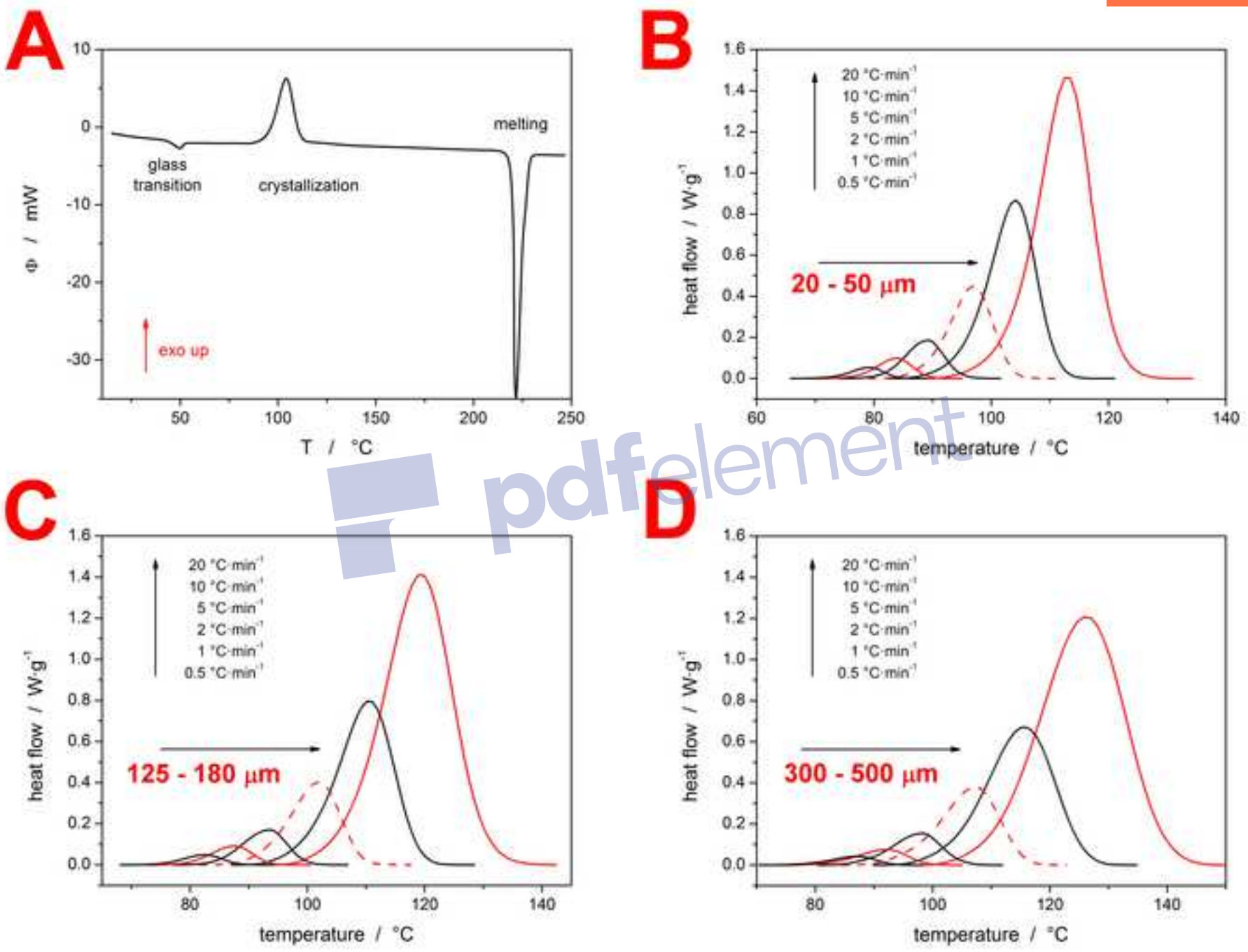

Figure 2

Click here to download high resolution image

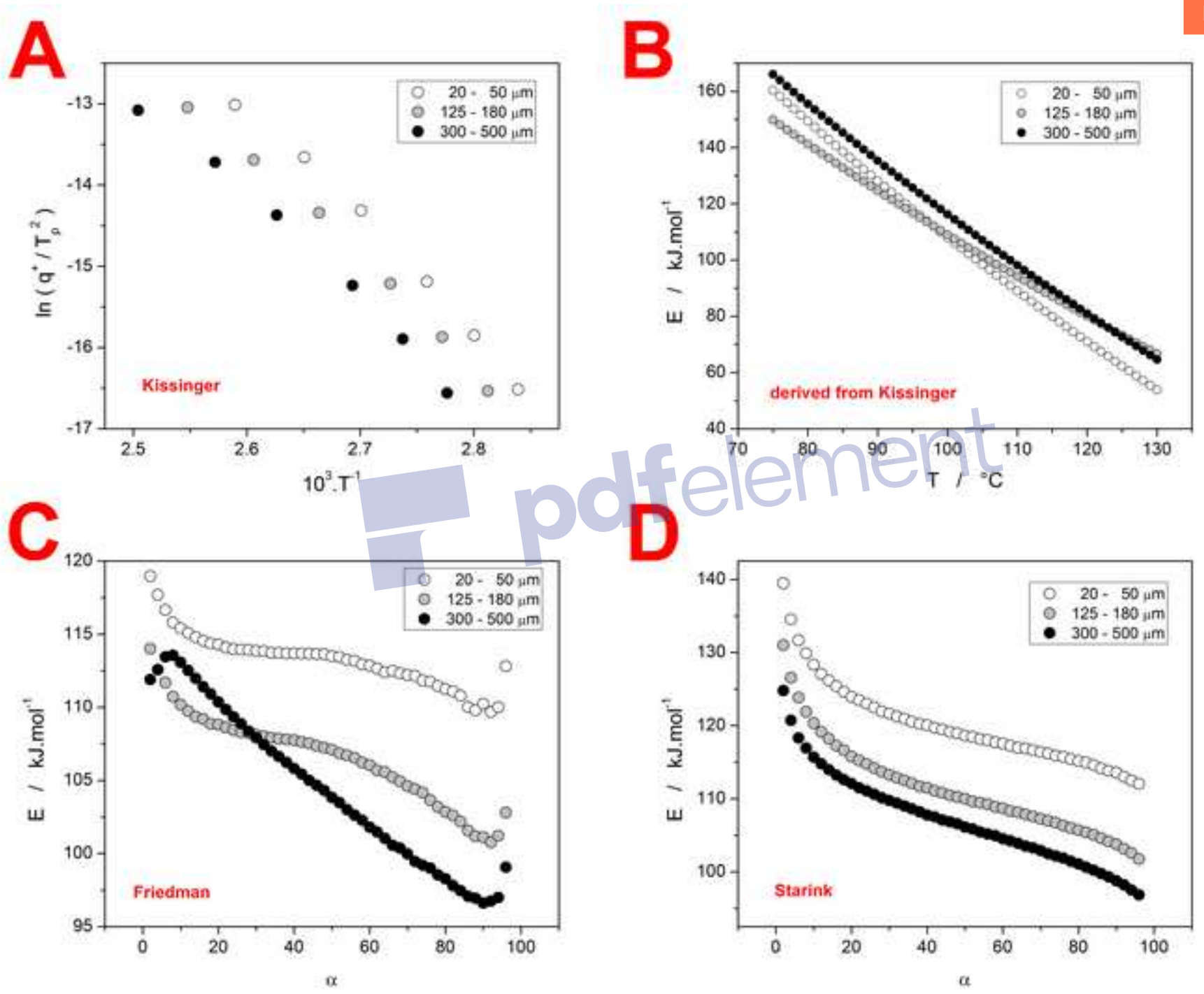

Figure 3

Click here to download high resolution image

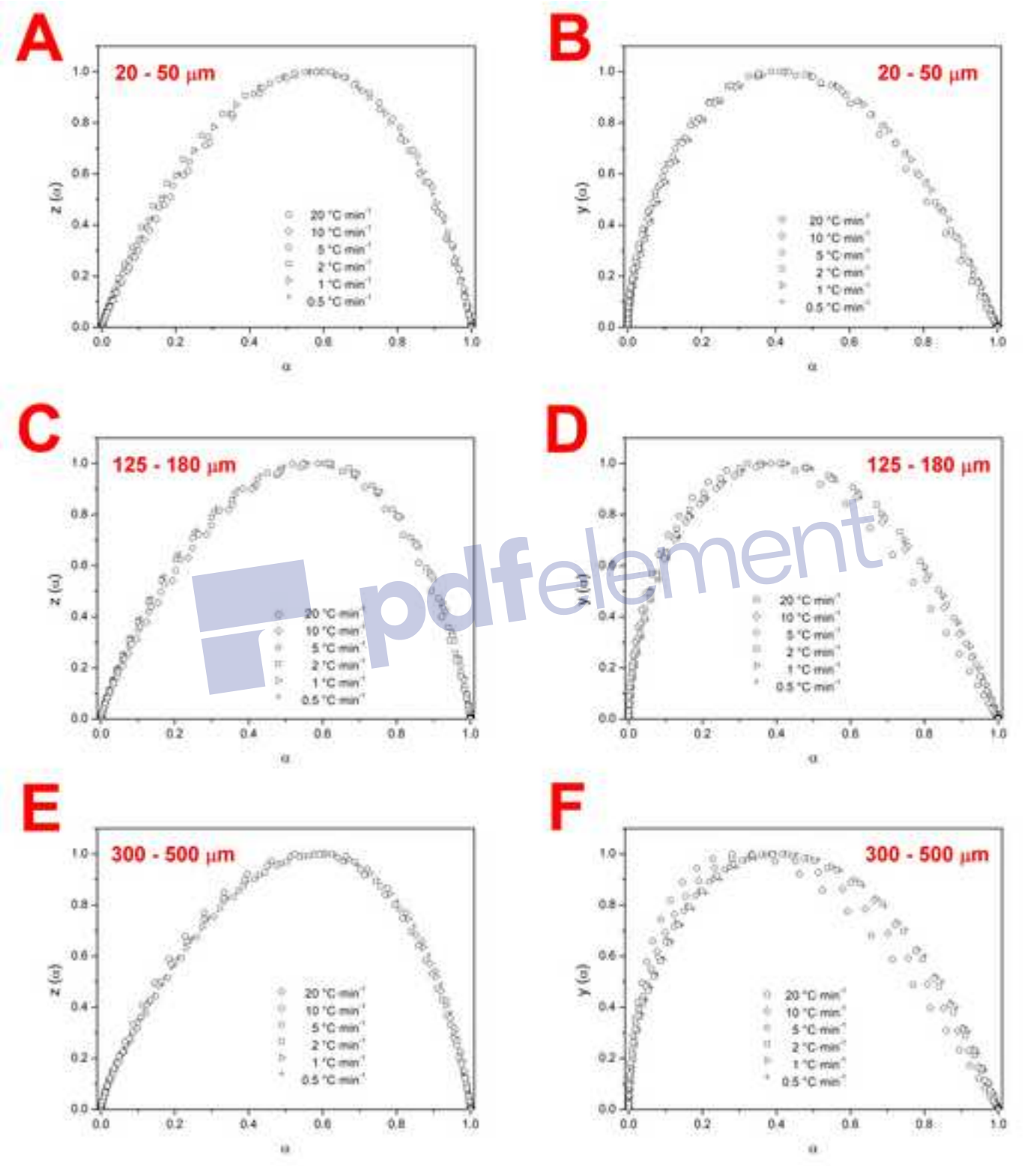

Figure 4

Click here to download high resolution image

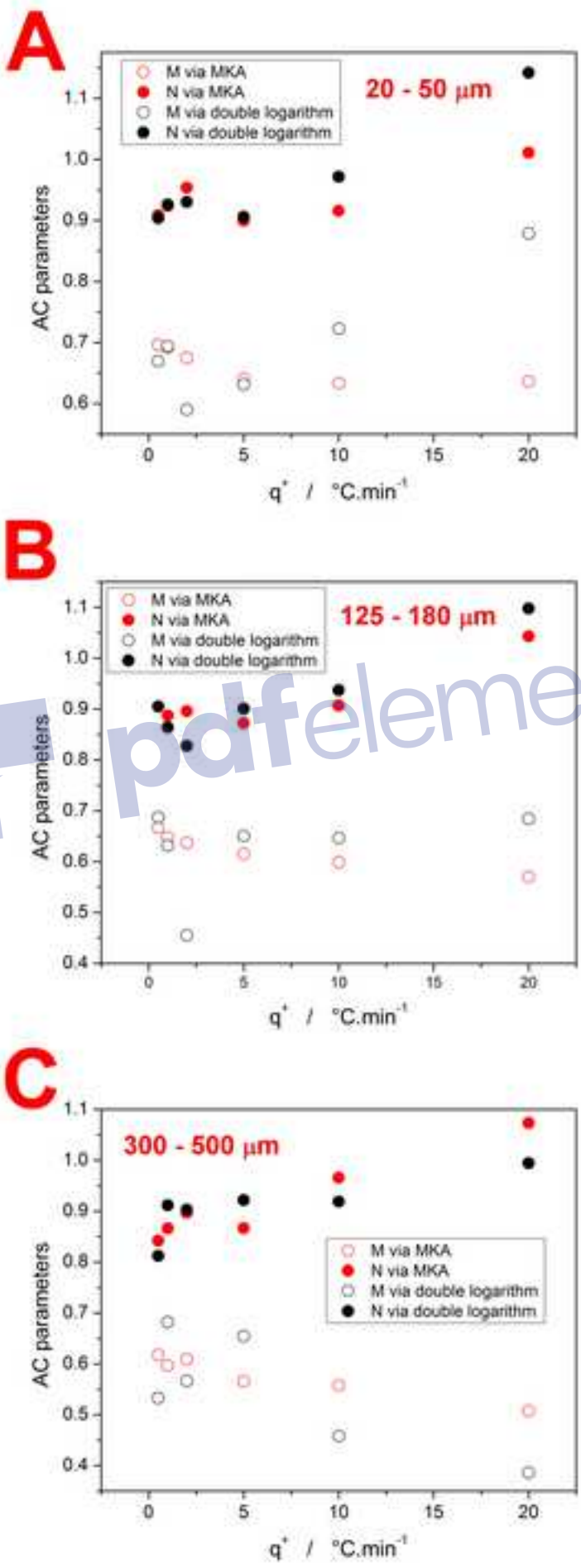

Figure 5

Click here to download high resolution image

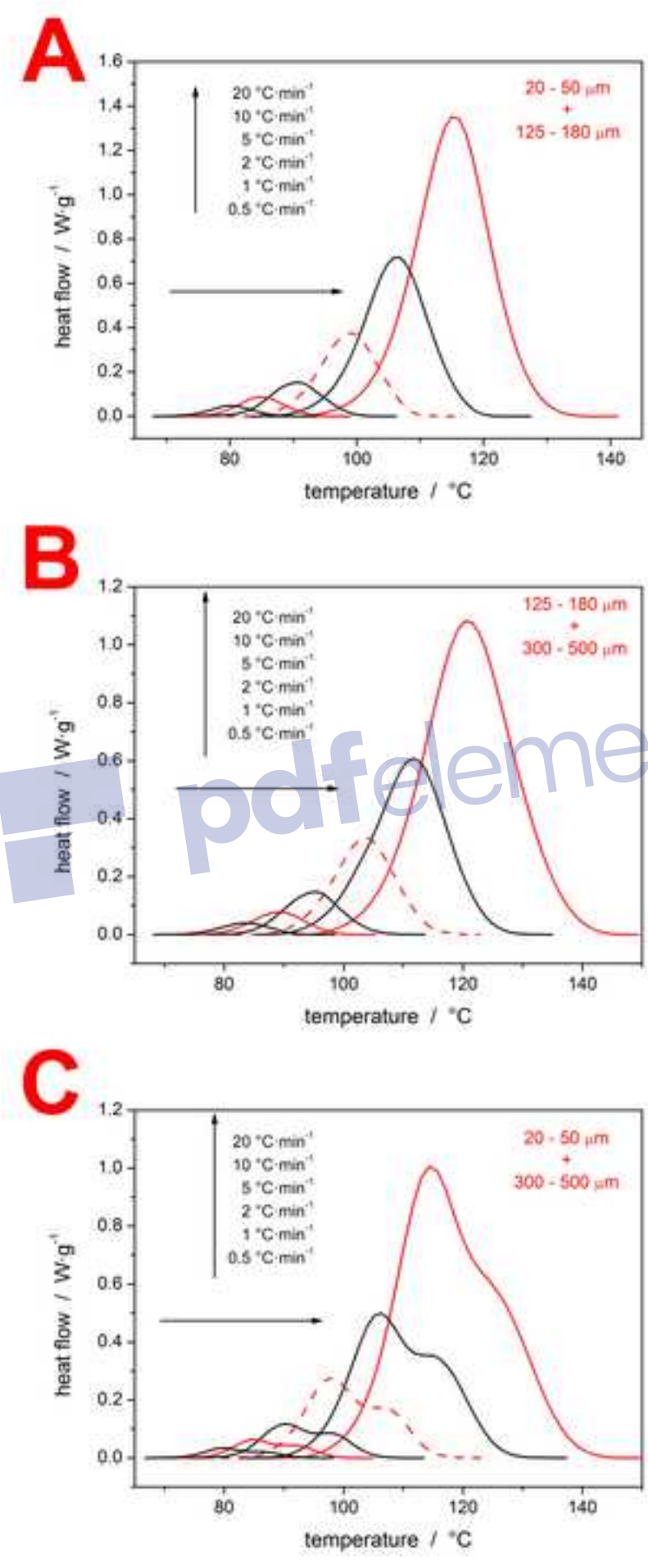

Figure 6

Click here to download high resolution image

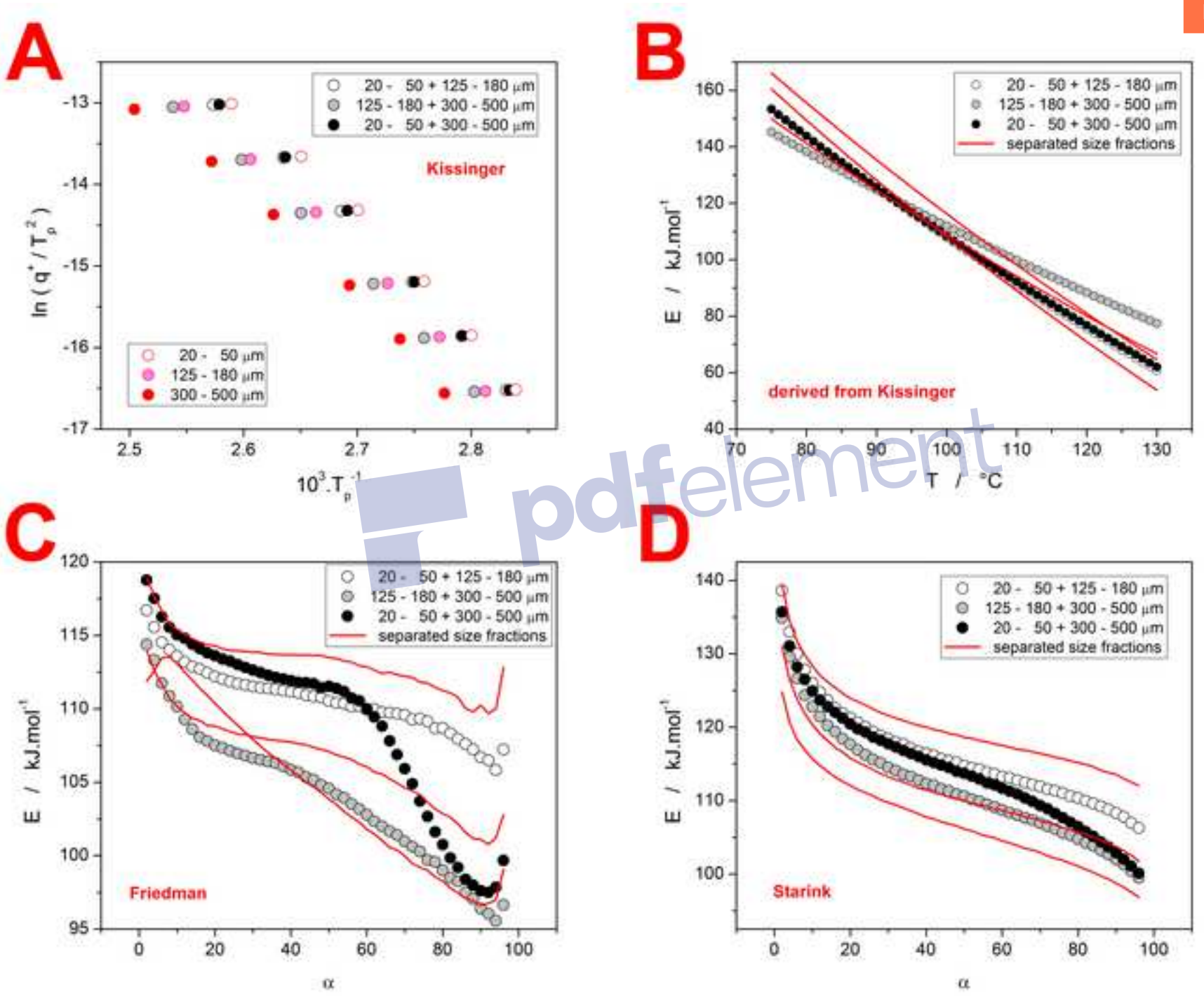

Figure 7

Click here to download high resolution image

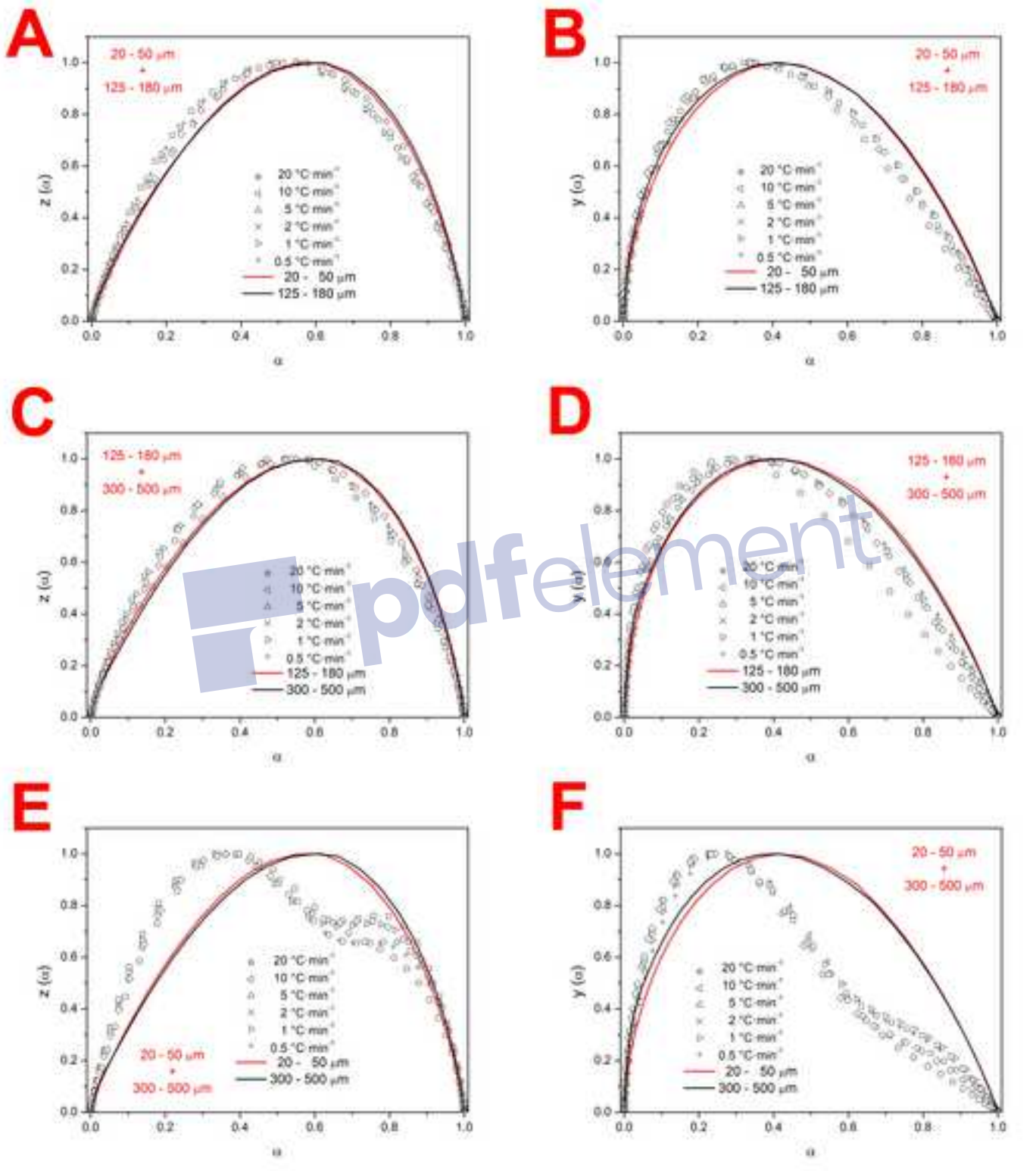

Figure 8

Click here to download high resolution image

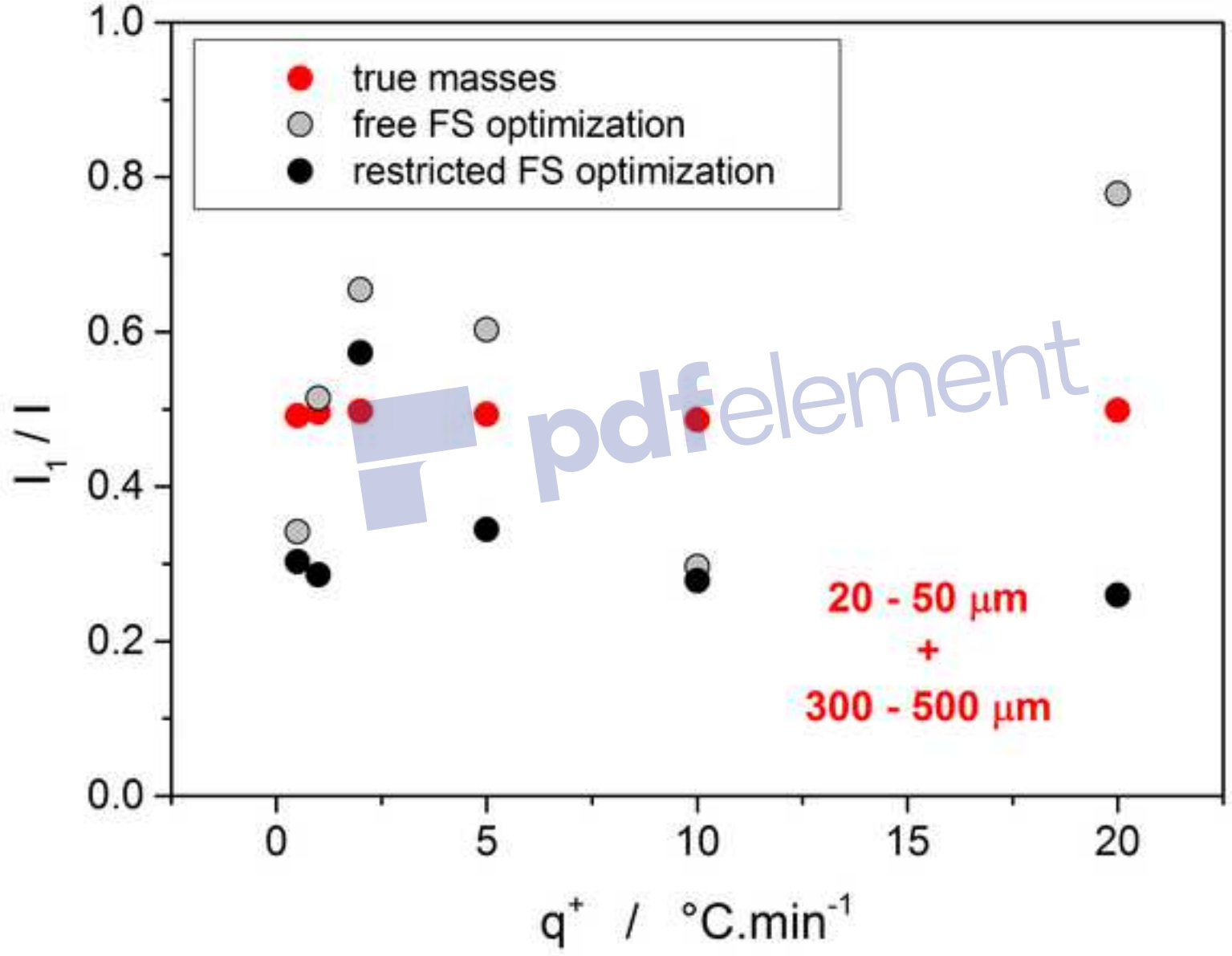

Figure 9

Click here to download high resolution image

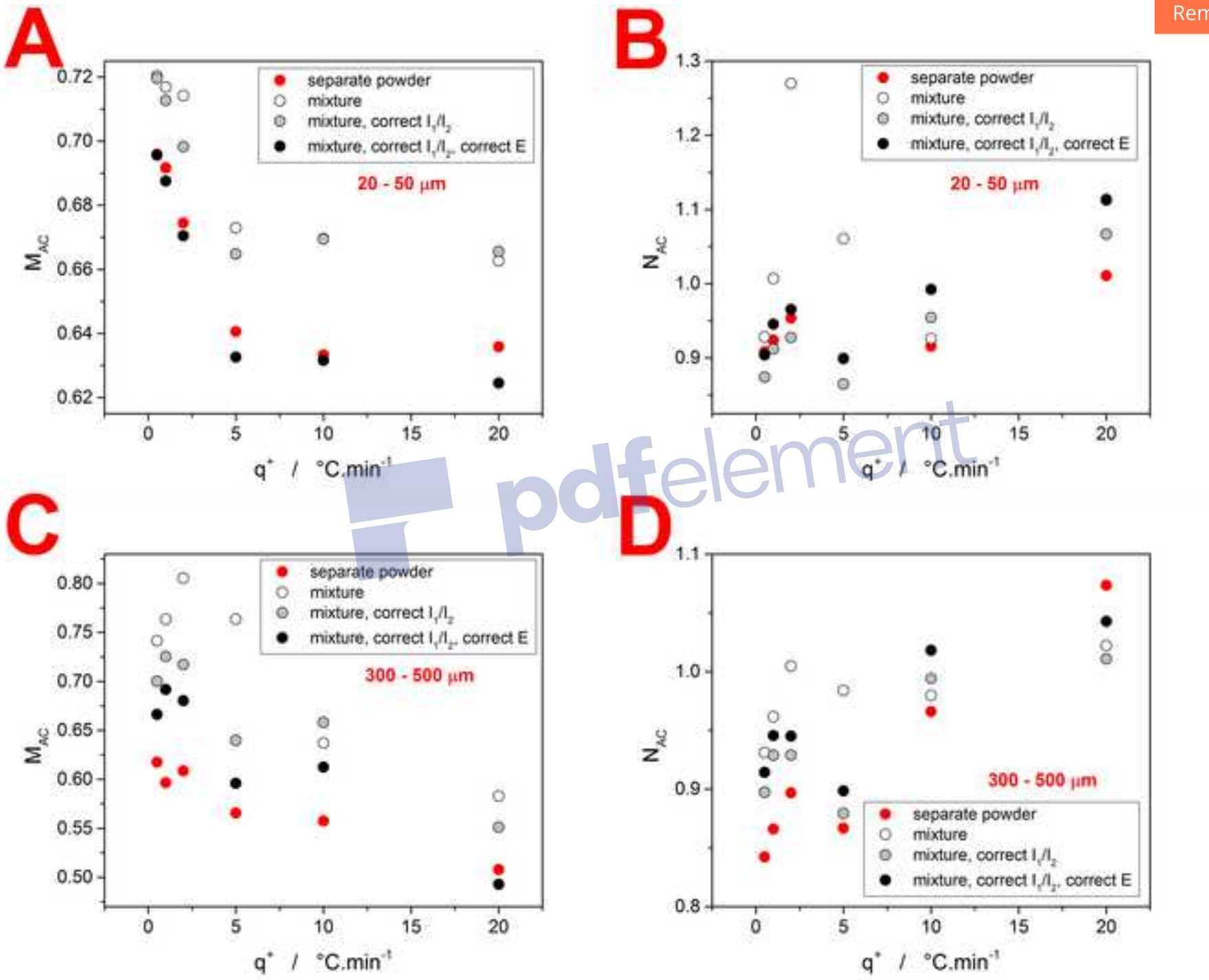

Figure 10

Click here to download high resolution image

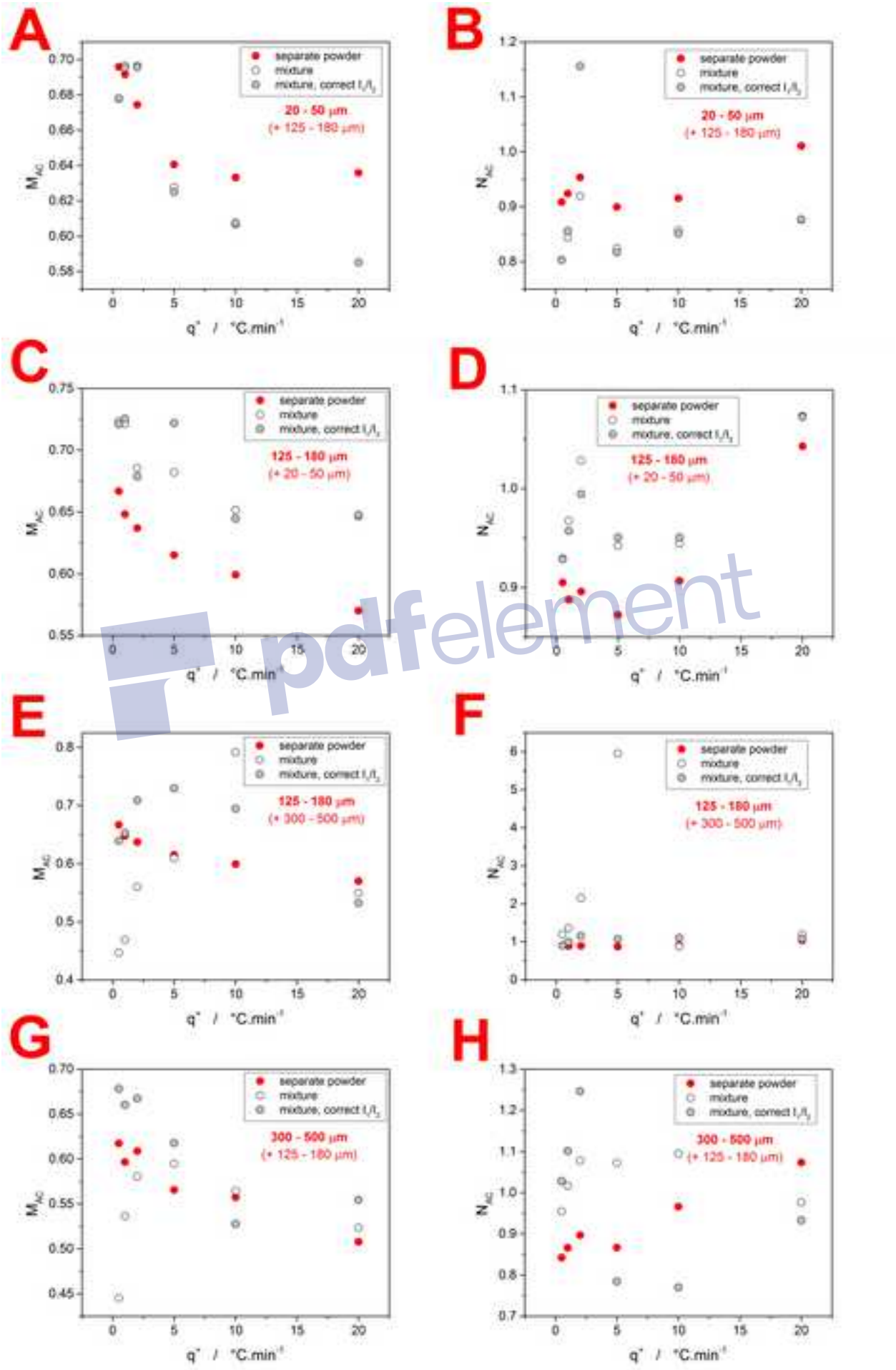

Figure 11

Click here to download high resolution image